Global jumping and domain-specific intersegment transfer between DNA cognate sites of the multidomain transcription factor Oct-1

Michaeleen Doucleff and G. Marius Clore†

Laboratory of Chemical Physics, National Institute of Diabetes and Digestive and Kidney Diseases, National Institutes of Health, Bethesda, MD 20892-0520

Edited by Alan R. Fersht, University of Cambridge, Cambridge, United Kingdom, and approved July 17, 2008 (received for review May 27, 2008)

At high DNA concentration, as found in the nucleus, DNA-binding proteins search for specific binding sites by hopping between separate DNA strands. Here, we use $^{15}N_z$-exchange transverse relaxation optimized NMR spectroscopy to characterize the mechanistic details of intermolecular hopping for the multidomain transcription factor, human Oct-1. Oct-1 is a member of the POU family of transcription factors and contains two helix–turn–helix DNA-binding domains, POU_{HD} and POU_S, connected by a relatively short flexible linker. The two domains were found to exchange between specific sites at significantly different rates. The cotranscription factor, Sox2, decreases the exchange rate and equilibrium dissociation constant for Oct-1 ≥5-fold and ≈20-fold, respectively, by slowing the exchange rate for the POU_S domain. DNA-dependent exchange rates measured at physiological ionic strength indicate that the two domains use both an intersegmental transfer mechanism, which does not involve the intermediary of free protein, and a fully dissociative or jumping mechanism to translocate between cognate sites. These data represent an example of dissecting domain-specific kinetics for protein–DNA association involving a multidomain protein and provide evidence that intersegmental transfer involves a ternary intermediate, or transition state in which the DNA-binding domains bridge two different DNA fragments simultaneously.

intermolecular translocation | protein–DNA interaction | $^{15}N_2$-exchange NMR spectroscopy | domain-specific kinetics | target searching

For ≈30 years biochemists have known that transcription factors locate their specific target sites faster than the simple three-dimensional diffusion-limited rate (1), but the details for this search process are still largely unknown. Three mechanisms are believed to facilitate the target search process (2–4): sliding, jumping, and intersegmental transfer. Sliding involves initial nonspecific binding of the protein followed by one-dimensional diffusion along the DNA. In the case of jumping, the protein dissociates from the DNA, diffuses briefly in free solution, and then reassociates a short distance along the DNA. Finally, intersegmental transfer comprises direct translocation of the protein between distant sites (separated >150 bp) by binding transiently to two separate DNA fragments brought together by looping or chromosomal packing. This type of intermolecular exchange through a "bridged" complex is also known as "direct" transfer (5–7).

Recent studies on sliding or jumping have provided insights into the kinetics (8, 9), structural properties (10), and relative populations (11) for these two facilitated-diffusion mechanisms. In comparison, less is known about intersegmental transfer, although recent theoretical studies predict that this mechanism significantly accelerates the target search process under conditions where the protein spends much of its time adsorbed on DNA, as is likely to be the case *in vivo* (5). Prior intersegmental transfer studies treated the proteins globally, obscuring mechanistic details specific to protein regions or domains (12–14). Here, we use $^{15}N_z$-exchange NMR spectroscopy (15) to characterize domain-specific details of intersegmental transfer for a multidomain transcription factor, namely the POU family protein, Oct-1.

The POU proteins are key transcription regulators during mammalian development, and, in addition, they control many general cellular processes. For example, Oct-1 activates expression of the HoxB1 transcription factor during neural development (16) and also regulates cell growth, differentiation, and survival in many tissues throughout a human lifetime (17). POU proteins have two DNA-binding domains: the specific domain known as POU_S and a homeodomain called POU_{HD}. These two helix–turn–helix motifs are connected by a flexible linker (≈23 aa long) (Fig. 1 *A* and *B*) and recognize specific binding sequences (red and blue lines above DNA_A in Fig. 1*B*).

Here, we present domain-specific kinetic data for protein–DNA association involving a multidomain transcription factor. The two tethered DNA-binding domains of Oct-1 translocate between high-affinity binding sites at significantly different rates. DNA-dependent data show that Oct-1 uses both jumping and intersegmental transfer mechanisms to exchange between its cognate sites. Together, these results provide evidence that intersegmental transfer involves a ternary intermediate or transition state in which the DNA-binding domains bridge two different DNA fragments simultaneously.

Results and Discussion

POU_S Exchanges Between DNA_A and DNA_B Significantly Faster than POU_{HD}. To measure how fast Oct-1 transfers between two high-affinity sequences, we used an experimental design similar to that described by Iwahara and Clore (18). We changed 1 bp between the POU_S and POU_{HD} recognition sites in the *HoxB1* promoter to create DNA_A and 1 bp at the other edge of the POU_{HD} recognition site to create DNA_B (Fig. 1*B*). These modifications minimally affect the affinity of Oct-1 for *HoxB1* DNA, but they do change the ^1H–^{15}N chemical shifts for several backbone amide groups in the Oct-1·DNA_A and Oct-1·DNA_B complexes (referred to hereafter as complexes A and B, respectively).

Oct-1 binds extremely tightly to its cognate DNA sequences with equilibrium dissociation constants K_{diss} ranging from 10^{-11} to 10^{-8} M (19). Not surprisingly, the ^1H–^{15}N transverse relaxation optimized (TROSY) correlation spectrum for a 1:1 mixture of complexes A and B contains peaks from both binary complexes (Fig. 1*C Left*), indicating that the apparent exchange rates for Oct-1 between complexes A and B are slow compared with

Author contributions: M.D. and G.M.C. designed research; M.D. performed research; M.D. and G.M.C. analyzed data; M.D. and G.M.C. wrote the paper.

The authors declare no conflict of interest.

This article is a PNAS Direct Submission.

†To whom correspondence should be addressed. E-mail: mariusc@mail.nih.gov.

This article contains supporting information online at www.pnas.org/cgi/content/full/0805050105/DCSupplemental.

BIOPHYSICS

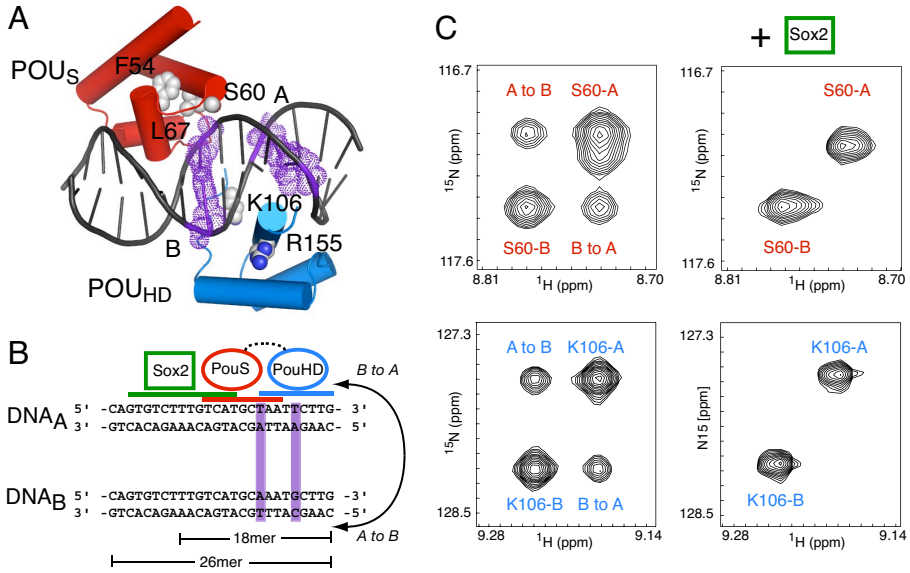

Fig. 1. Intermolecular exchange between Oct-1·*HoxB1* DNA complexes. (*A*) X-ray crystal structure (Protein Data Bank ID code 1OCT) (29) of Oct-1 (POU_S in red and POU_{HD} in blue) in complex with promoter DNA. Exchange rates were determined for the five residues labeled and represented as spheres: F54, L67, and S60 in the POU_S domain, and K106 and R155 in the POU_{HD} domain. The purple mesh identifies the base pairs changed in DNA_A and DNA_B. (*B*) *HoxB1* DNA fragments, DNA_A and DNA_B, differing by 2 bp (purple box). Solid lines above DNA_A indicate the binding regions for each element of the Oct-1·*HoxB1*·Sox2 ternary complex (24). The 18-mer and 26-mer DNA duplexes were used for $^{15}N_z$-exchange experiments on Oct-1·*HoxB1* and Oct-1·*HoxB1*·Sox2 complexes, respectively. (*C*) Example of exchange data for S60 of POU_S (*Upper*) and K106 of POU_{HD} (*Lower*) in the ^1H–^{15}N TROSY-based *z*-exchange spectrum. Example data for the Oct-1·*HoxB1* binary and Oct-1·*HoxB1*·Sox2 ternary complexes are shown on the *Left* and *Right*, respectively.

the chemical shift time scale (k_{AB}^{app} and $k_{BA}^{app} \ll \omega_A - \omega_B \approx 300\ s^{-1}$).

If the Oct-1 domains transfer between DNA_A and DNA_B (or vice versa) during a *z*-mixing period (<800 ms) inserted into the pulse scheme after ^{15}N t_1 evolution, exchange cross-peaks will be visible in a ^1H–^{15}N TROSY-based $^{15}N_z$-exchange experiment (20). The *z*-mixing period includes an S scheme to eliminate the buildup of spurious semi-TROSY peaks (20). At low salt concentrations (10 mM phosphate buffer), no cross-peaks were detected (data not shown). At physiological salt concentrations (150 mM NaCl), however, cross-peaks are clearly apparent for residues in both the POU_S and POU_{HD} domains (Fig. 1*C Left*). This correlation between intermolecular exchange rate and ionic strength has been observed for both protein–DNA (10, 21) and protein–protein complexes (22).

By varying the length of the *z*-mixing period and then fitting the cross-peak and autopeak intensities to the McConnell equations (23) describing a simple first-order exchange scheme [supporting information (SI) Fig. S1*A*], we determined the apparent exchange rates, k_{AB}^{app} and k_{BA}^{app}, for five Oct-1 residues: F54, S60, and L67 in POU_S; and K106 and R155 in POU_{HD} (labeled spheres in Fig. 1*A*). These were the only Oct-1 residues with at least three well dispersed, analyzable auto- and cross-peaks in the ^1H–^{15}N TROSY-based $^{15}N_z$-exchange experiment. A plot of the apparent rates for these residues vs. temperature (25, 30, and 35°C) clearly shows that the exchange rates segregate by domain (Fig. S2). At all three temperatures, the average POU_S exchange rate is 1.4–1.5 times faster than the average POU_{HD} exchange rate. A two-way ANOVA with temperature and domain as factors indicates that the domain effect is significant (with $P = 0.01$).

At each temperature, the data for the three POU_S residues fit well to a single set of k_{AB}^{app} and k_{BA}^{app} rate constants, and the data for the two POU_{HD} residues fit well to a significantly lower set of k_{AB}^{app} and k_{BA}^{app} rate constants. For example, at 30°C, $k_{AB}^{app} = 4.26 \pm 0.06\ s^{-1}$ and $k_{BA}^{app} = 4.54 \pm 0.07\ s^{-1}$ for POU_S (χ^2 per degree of freedom = 1.12), whereas $k_{AB}^{app} = 2.90 \pm 0.06\ s^{-1}$ and $k_{BA}^{app} = 3.06 \pm 0.06\ s^{-1}$ for POU_{HD} (χ^2 per degree of freedom = 1.12) (Fig. 2 *A* and *B*, respectively). In contrast, fitting the data from both domains to global k_{AB}^{app} and k_{BA}^{app} yields a poor fit with a value of 2.77 for χ^2 per degree of freedom.

Addition of the Coactivator Sox2 Slows Exchange Rates for Both POU_S and POU_{HD}. Eukaryotic transcription factors invariably act in concert with multiple cofactors to achieve cell-specific transcription regulation. For example, Oct-1 alone can stimulate transcription of the *HoxB1* gene, but maximum transcription activity requires both Oct-1 and the cofactor Sox2 (shown in green in Fig. 1*B*), which increases Oct-1-directed transcriptional activation by 40% (16). To determine how cofactors affect the intermolecular transfer rates of Oct-1, we repeated the exchange experiments in the presence of Sox2 with longer DNA fragments that include the Sox2-binding site (Fig. 1*B*).

Sox2 dramatically decreases the translocation rates for both POU_S and POU_{HD}. No cross-peaks are detectable for either domain translocating between Oct-1·*HoxB1*·Sox2 ternary complexes (Fig. 1*C Right*) under identical conditions where cross-peaks are clearly visible for transfer between Oct-1·*HoxB1* binary complexes (Fig. 1*C Left*). Even at higher ionic strength and temperature (250 mM NaCl at 40°C), cross-peaks for POU_S and POU_{HD} in the ternary complexes are barely detectable at mixing times >150 ms (data not shown). Consistent with this change in kinetics, Sox2 also increases the affinity of Oct-1 for the *HoxB1* promoter by almost 20-fold, decreasing K_{diss} from 16.3 ± 0.4 nM to 0.9 ± 0.2 nM (Fig. S3).

The minimum exchange rate measurable by $^{15}N_z$-exchange spectroscopy depends on longitudinal relaxation time ^{15}N-T_1, with $k_{min} \approx 1/^{15}N\text{-}T_1$ (15). With a ^{15}N-$T_1 \approx 1$ s for Oct1·*HoxB1*·Sox2 at 37°C (data not shown), we estimate the exchange rate of Oct-1 between ternary complexes to be $<1\ s^{-1}$ and, therefore, at least 5-fold slower than the exchange rate between Oct-1·*HoxB1* binary complexes.

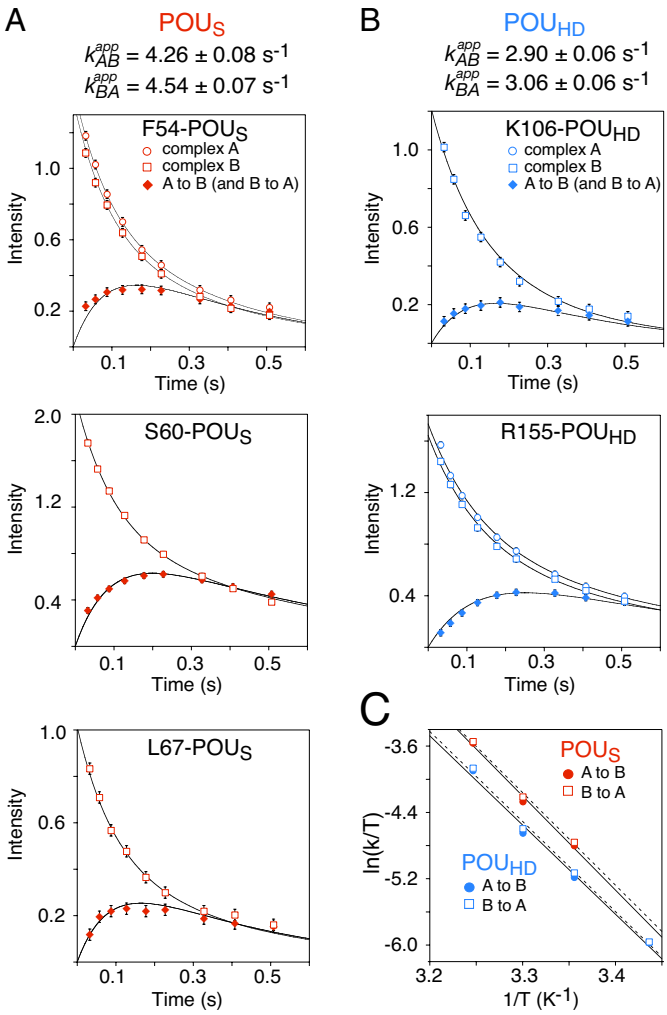

Fig. 2. POU_S exchanges between specific DNA binding sites significantly faster than POU_{HD}. At each temperature, 25, 30, and 35°C (and 18°C POU_{HD}), all data for each domain were fit simultaneously, and the apparent first-order intermolecular exchange rates were determined. Examples of the measured cross-peak (solid diamonds) and autopeak (open squares and circles) intensities at 30°C together with the best-fit curves for residues from the POU_S and POU_{HD} domains are shown in *A* and *B*, respectively. The experimental data for the cross-peaks represent the average of the data for the two symmetry-related cross-peaks. The calculated domain-specific rate constants at 30°C are shown above the graph. (*C*) Erying plots of the average apparent exchange rates for POU_S (red) and POU_{HD} (blue) at 25, 30, and 35°C and for POU_{HD} at 18°C. Linear fits for the exchange rates from A to B (k_{AB}^{app}) and from B to A (k_{BA}^{app}) are shown as solid lines and dotted lines, respectively; activation enthalpies and entropies derived from the data are provided in Table 1.

In the NMR structure of the *Oct-1·HoxB1·Sox2* ternary complex, Sox2 contacts only the POU_S domain of Oct-1 (24). This structure, combined with our exchange data, shows that Sox2 kinetically traps Oct-1 at the *HoxB1* promoter by slowing the transfer between DNA-specific sites of the faster POU_S domain, thereby leading to a global decrease in the exchange rate of Oct-1. These data also indicate that the intermolecular transfer for the two domains is not completely independent but partially coupled, which is expected for tethered domains that bind to DNA with a small amount of cooperativity ($\Delta\Delta G = -1.6$ kcal·mol^{-1}) (25).

Activation Barrier for Intersegmental Exchange Is Enthalpic. Erying plots of the temperature-dependent apparent exchange rates (Fig. 2*C*) estimate that the activation enthalpy ($\Delta H^{\ddagger}$) and activation entropy ($T\Delta S^{\ddagger}$ at 30°C) for the intermolecular exchange of Oct-1 are ≈22 and ≈5 kcal·mol^{-1}, respectively. Therefore, the energetic barrier for the transfer of Oct-1 between high-affinity sites is primarily enthalpic, just as found for the intermolecular exchange for the single helix–turn–helix motif HoxD9 homeodomain ($\Delta H^{\ddagger} = 17.1$ kcal·mol^{-1} and $T\Delta S^{\ddagger} = 1.17$ kcal·mol^{-1} at 30°C) (20). This finding is not surprising given that both POU domains and the HoxD9 homoedomain bind in the major groove (Fig. 1*A*), which is typically associated with a negative enthalpy and a slightly positive entropy (26).

Table 1. Apparent activation enthalpies, entropies, and free energies for intermolecular translocation of Oct-1 between specific DNA-binding sites

Transfer process	$\Delta H^{\ddagger}$, kcal·mol^{-1}	$T\Delta S^{\ddagger}$, kcal·mol^{-1}	$\Delta G^{\ddagger}$*, kcal·mol^{-1}
POU_S			
A to B	22.6 ± 2.1	5.6 ± 2.1	16.9
B to A	22.2 ± 1.5	5.3 ± 1.5	16.9
POU_{HD}			
A to B	21.4 ± 1.4	4.3 ± 1.4	17.1
B to A	21.6 ± 1.1	4.5 ± 1.1	17.1

Values were derived by least-squares fitting from the Eyring plots shown in Fig. 2*C*. The values given for $T\Delta S^{\ddagger}$ are at a temperature of 298 K. $\Delta G^{\ddagger}$ is calculated from $\Delta G^{\ddagger} = \Delta H^{\ddagger} - T\Delta S^{\ddagger}$ at 298 K.
*The calculated error for each $\Delta G^{\ddagger}$ value is less than 0.01 kcal·mol^{-1}.

Oct-1 Exchanges Between Binding Sites Using Both Jumping and Intersegmental Transfer. DNA-binding proteins can translocate between specific sites, which are located either on two separate DNA fragments or far apart on a single piece of DNA, by using two mechanisms: (*i*) jumping or hopping that involves a fully dissociated protein as an intermediate (Fig. 3 *Lower*), and (*ii*) direct intersegmental transfer that involves a ternary intermediate, in which the protein binds simultaneously to two fragments of DNA (Fig. 3 *Upper*). Two possible ternary intermediates or transition states for Oct-1 intersegmental transfer are designated with yellow stars in Fig. 3.

These mechanisms lead to different rate dependences on free DNA concentration. Under the experimental conditions used ($k_{on}^{A} \approx k_{on}^{B}$, $[DNA_A^{free}] = [DNA_B^{free}]$ and $k_{off} \ll k_{on}[DNA^{free}]$), the apparent exchange rates (k_{AB}^{app} and k_{BA}^{app}) through the fully dissociative pathway are independent of free DNA concentration and equal to $k_{off}^{A}/2$ and $k_{off}^{B}/2$ for exchange from A to B and from B to A, respectively (for a derivation of this equation, see Fig. S4). In contrast, for the intersegmental pathway, the apparent exchange rates k_{AB}^{app} and k_{BA}^{app} are directly proportional to the free DNA concentration with $k_{AB}^{app} = k_{AB}^{*}[DNA_B^{free}]$ and $k_{BA}^{app} = k_{BA}^{*}[DNA_A^{free}]$, where k_{AB}^{*} and k_{BA}^{*} are second-order rate constants.

The apparent exchange rates for both POU_S and POU_{HD} scale linearly with free DNA concentration (all correlation coefficients $r > 0.99$ in Fig. 4), indicating that Oct-1 must use the second-order intersegmental pathway to exchange between complexes A and B (Fig. 3 *Upper*). However, this mechanism alone does not fully account for the DNA-dependent data because exchange via the intersegmental transfer mechanism is expected to be zero in the absence of free DNA. The intercepts of the regression lines in Fig. 4 clearly do not pass through the origin, indicating a contribution from the fully dissociative mechanism (Fig. 3 *Lower*). A global fit to the time-dependent $^{15}N_z$-exchange data at all DNA concentrations simultaneously while optimizing domain-specific, second-order intersegment transfer rate constants together with global dissociation and association rate constants yields a χ^2 per degree of freedom of 0.9 (for model details, see Fig. S1*B*).

BIOPHYSICS

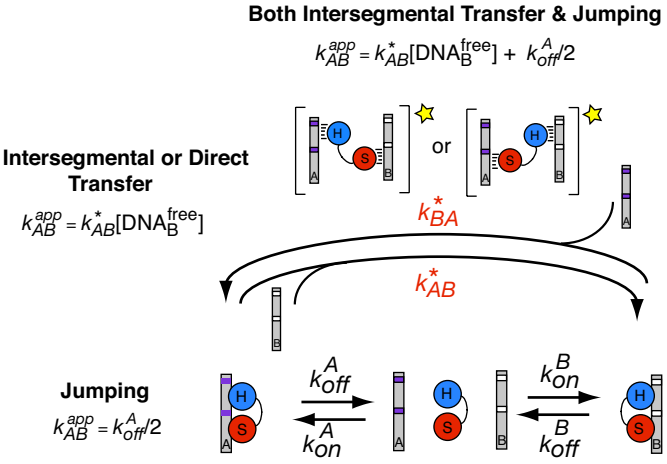

Fig. 3. Oct-1 exchanges between complexes A and B using two different mechanisms, intersegmental transfer and jumping. In the jumping mechanism (*Lower*), both POU domains fully dissociate from DNA_A before binding to DNA_B (and vice versa); under the experimental conditions used (see *Results and Discussion* and Fig. S4), the transfer rates between DNA-binding sites for the jumping mechanism are independent of DNA concentration and depend only on the global dissociation rate constants: $k_{AB}^{app} = k_{off}^{A}/2$ and $k_{BA}^{app} = k_{off}^{B}/2$ (for derivation, see Fig. S4). In the intersegmental transfer pathway (*Upper*), the POU domains interact simultaneously with two DNA fragments, creating two possible ternary intermediates or transition states (yellow stars); the apparent rate constants through this pathway are directly proportional to the free DNA concentrations. When both mechanisms are operative, the apparent rate constant $k_{AB}^{app} = k_{AB}^{*}[DNA_B^{free}] + k_{off}^{A}/2$ and similarly, $k_{BA}^{app} = k_{BA}^{*}[DNA_A^{free}] + k_{off}^{B}/2$.

At 30°C, Oct-1 fully dissociates from DNA_A with a dissociation rate constant $k_{off}^{A} = 3.73 \pm 0.19\ s^{-1}$ and from DNA_B with $k_{off}^{B} = 5.09 \pm 0.26\ s^{-1}$; Oct-1 binds to both fragments with an association rate constant $k_{on} = 2.34(\pm 0.12) \times 10^8\ M^{-1}\ s^{-1}$ (note, k_{on}^{A} and k_{on}^{B} are assumed to be equal because the data cannot determine individual values for these two rate constants). The second-order intersegmental transfer rate constants for the POU_S domain are ≈1.6 times faster than those for the POU_{HD} domain: $k_{AB}^{S*} = 2.88(\pm 0.10) \times 10^4\ M^{-1}\ s^{-1}$ vs. $k_{AB}^{HD*} = 1.85(\pm 0.08) \times 10^4\ M^{-1}\ s^{-1}$ for exchange from A to B, and $k_{BA}^{S*} = 3.92(\pm 0.13) \times 10^4\ M^{-1}\ s^{-1}$ vs. $k_{BA}^{HD*} = 2.52(\pm 0.11) \times 10^4\ M^{-1}\ s^{-1}$ for exchange from B to A.

Concluding Remarks. Here, we present domain-specific kinetic data for intermolecular translocation of a multidomain transcription factor between specific DNA-binding sites. Almost 25 years ago, Fried and Crothers (14) showed that the exchange rate for the *lac* repressor scaled linearly with free DNA concentration, indicating a direct intersegmental transfer mechanism. This work and a subsequent one on the glucocorticoid receptor (13) implied the existence of, but were unable to detect, different rates for specific dimeric subunits (on nonsymmetric DNA-binding sites) because only global dissociation rates could be determined by gel mobility shift assays. The $^{15}N_z$-exchange data presented here provide the means to measure distinct transfer rates for tethered domains of a transcription factor and, thus, demonstrate direct evidence for a transient intermediate in which the protein interacts specifically with two DNA fragments (Fig. 3 *Upper*, yellow stars).

One biological function for the different intermolecular transfer rates of the POU_S and POU_{HD} domains may be to increase the efficiency of the Oct-1 target search process inside the nucleus. With a 1.5-fold faster exchange rate than POU_{HD}, POU_S could scan binding sequences on different DNA fragments, while POU_{HD} remains in complex with a high-affinity sequence, ensuring that global Oct-1 exchange only occurs when POU_S identifies another cognate binding site. The details of this search mechanism could potentially be characterized in future experiments by examining domain-specific interactions with nonspecific DNA by using paramagnetic relaxation enhancement to visualize transient interactions (10).

The different exchange rates of the POU DNA-binding domains may also contribute to the fine tuning of cell- and tissue-specific transcription regulation by Oct-1. Even when Oct-1 acts in concert with other cofactors, subtle changes in the Oct-1 promoter sequence or binding affinity *in vitro* can have large effects on gene expression *in vivo*. For example, Oct-1 together with the GATA-1 protein represses transcription of the human fetal globin genes in adults (27, 28). Only a single base pair mutation at the POU_{HD} hemisite reduces the DNA-binding affinity of Oct-1 and results in the diseased phenotype (28). In contrast, transcription activation of the *HoxB1* gene by Oct-1 with Sox2 depends only on the integrity of the POU_S-binding site (16). Therefore, different kinetic parameters for the POU_S and POU_{HD} domains at particular promoters may result in differential transcription activation or repression by Oct-1 cofactors, depending on whether they target the POU_S domain or POU_{HD} domain.

Our data indicate that at physiological ionic strength (150 mM NaCl), Oct-1 uses both jumping (i.e., complete dissociation followed by reassociation) and intersegmental transfer (i.e., direct transfer without the intermediary of free protein) to exchange between high-affinity DNA-binding sites *in vitro* (Fig. 3). At a free DNA concentration of 150 μM, the fully dissociative pathway accounts for ≈25% of the apparent exchange rate for Oct-1 (Fig. 4). In contrast, jumping did not contribute significantly to the exchange rate for the single helix–turn–helix homeodomain HoxD9 (18). This difference is probably because, under the experimental conditions used, Oct-1 binds to the HoxB1 DNA promoter (K_{diss} = 16.3 nM) 10 times weaker than HoxD9 binds to its cognate DNA site ($K_{diss} < 1.5$ nM), making the dissociative pathway for Oct-1 energetically comparable with the intersegmental transfer mechanism. In support of this conclusion, the Arrhenius-like equation $k_{off} = (k_B T/h)\ \exp^{(\Delta G^{\ddagger}/RT)}$ with $k_{off} \approx 5\ s^{-1}$ at 30°C predicts an activation free energy ($\Delta G^{\ddagger}$) of ≈17 kcal·mol^{-1} for full dissociation of Oct-1 from DNA, which is exactly the activation free energy we measured for the Oct-1 overall exchange process (Table 1).

Because the data from both domains fit well to the same global dissociation constants (k_{off}^{A} and k_{off}^{B}), the different exchange rates observed for POU_S and POU_{HD} (Fig. 2) must arise from an asymmetry in the intersegmental exchange pathway (Fig. 3 *Upper*). Expressed as isolated protein fragments, POU_S and POU_{HD} bind with significantly different affinities to promoter sites. For example, POU_{HD} binds 150 times tighter than POU_S

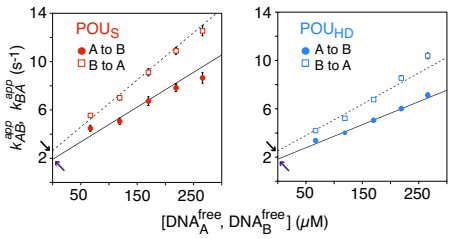

Fig. 4. Apparent exchange rates at five free DNA concentrations for POU_S (*A*) and POU_{HD} (*B*). Apparent exchange rates from A to B (k_{AB}^{app}) and from B to A (k_{BA}^{app}) are shown as filled circles and open squares, respectively. Black lines represent the theoretical rate dependence on free DNA concentration obtained by simultaneously fitting all of the data for the two domains to a model comprising the intersegmental transfer mechanism in parallel with the jumping mechanism (as shown in Fig. 3 and Fig. S1*B*). Purple and black arrows point to the *y* intercepts, which equal $k_{off}^{A}/2$ and $k_{off}^{B}/2$, respectively.

to the human *H2B* histone promoter, which has a sequence similar to that of *HoxB1* (25). Therefore, the binary Oct-1·*HoxB1* DNA complexes are probably not static structures as seen in x-ray crystal structures (29, 30) but are possibly in rapid dynamic equilibrium with hemiassociated states, in which only one domain contacts the DNA. The detached domain would then be accessible to transfer directly to free DNA via the intersegmental pathway, forming a bridged complex or transition state as shown in Fig. 3 *Upper* (yellow stars). An asymmetry in the population of these two ternary intermediates (Fig. 3 *Upper*, yellow stars) or the two possible hemidissociated states may lead to the different transfer rates observed for POU_S and POU_{HD} (Fig. 2). (Note that the kinetic scheme combining direct intersegmental transfer and jumping shown in Fig. S1*B* represents the simplest scheme required to account for the DNA concentration-dependent $^{15}N_z$-exchange data; the information content, however, in the time-dependent $^{15}N_z$-exchange data is insufficient to determine the much larger number of unknown parameters required to describe quantitatively more complex schemes explicitly including hemiassociated states or ternary intermediates.)

The intermolecular transfer mechanism presented here is likely applicable to many other important eukaryotic transcription factors that contain multiple DNA-binding domains connected by linkers, such as the Myb oncoproteins (31) and the Cys_2His_2 zinc finger proteins (32). All of these proteins have different linker lengths with various levels of structural order, so it will be interesting to determine how linker length and structure affect intermolecular transfer rates and mechanisms.

Materials and Methods

Sample Preparation of Oct1·DNA Complexes. The POU DNA-binding domains, POU_S and POU_{HD}, comprising residues 1–176 of human Oct-1 and the HMG box domain of human Sox2 (residues 40–123), were expressed and purified as described in ref. 24. Oct-1 was uniformly labeled with either ^{15}N–^{13}C–^{2}H (for triple resonance experiments to confirm assignments) or ^{15}N–^{2}H (for the $^{15}N_z$-exchange experiments). Oligonucleotides were purchased from Midland Certified Reagents or from the Yale University School of Medicine DNA Synthesis Laboratory (New Haven, CT). Single-stranded and duplex DNA fragments were purified by ion-exchange chromatography as described in ref. 18.

Before mixing, Oct-1 and DNA were desalted by dialysis or gel-filtration chromatography into 10 mM phosphate buffer (pH 6.5), 1 mM EDTA, and 3 mM DTT. Sox2 was dialyzed into 10 mM phosphate buffer (pH 6.5) and 1 mM EDTA. DNA and protein concentrations were measured from the absorbance at 260 and 280 nm, respectively. Concentrations were confirmed by gel-shift assays. All NMR samples were concentrated with an Amicon ultracentrifugal concentrator (3-kDa cutoff; Millipore Corporation) in buffer containing 5% D_2O, 10 mM phosphate buffer (pH 6.5), 10 mM DTT, and 1 × Complete protease inhibitor (Roche). Unless indicated otherwise, 150 mM NaCl was added to the sample immediately before data collection.

For the temperature dependence study, the NMR sample contained 550 μM U-[$^{2}H/^{15}N$]Oct-1, 350 mM DNA_A, and 350 mM DNA_B. For the DNA titration, the initial NMR sample (505 μl of total) contained 766 μM U-[$^{2}H/^{15}N$] Oct-1 with 450 μM DNA_A and 450 μM DNA_B. To increase the DNA concentration, we replaced 20 μl of the NMR sample with 20 μl of a stock solution containing 1.45 mM DNA_A and 1.45 mM DNA_B. For the ternary complex (Oct-1·*HoxB1*·Sox2), the sample contained 600 μM U-[$^{2}H/^{15}N$] Oct-1, 400 μM DNA_A, 400 μM DNA_B, and 800 μM Sox2.

K_{diss} Measurements. Equilibrium dissociation constants (K_{diss}) for Sox2 and Oct-1 at the *HoxB1* promoter were obtained by following changes in fluorescence anisotropy of labeled DNA upon titration with protein as described in ref. 18. For Oct-1 and Sox2 titrations, DNA was kept at 5 nM and 1.4 nM, respectively. Sox2 binding to *HoxB1* increased the anisotropy significantly more than Oct-1 binding (Fig. S3 *A* and *B*). We, therefore, determined the K_{diss} for Oct-1 in the presence of Sox2 by measuring K_{diss} for Sox2 in the presence of Oct-1 (Fig. S3*B*, filled circles). We then calculated the effect of Sox2 on the K_{diss} of Oct-1 by using a thermodynamic cycle (Fig. S3*C*).

NMR Spectroscopy. All NMR data were recorded on a Bruker DRX 800-MHz spectrometer equipped with a *z*-gradient triple resonance cryoprobe, at 30°C, unless specified otherwise. Data were processed with NMRPipe (33) and analyzed using CARA (www.nmr.ch) or NMRDraw (33). Backbone assignments for the Oct-1 POU domains (24) were confirmed with TROSY (34) versions of 3D HNCA, HNCO, and HN(CA)CO triple resonance experiments (35). Exchange rates were measured with a TROSY version of a 2D $^{15}N_z$-exchange ^{1}H–^{15}N correlation experiment incorporating an S scheme during the *z*-mixing period to eliminate the buildup of spurious semi-TROSY peaks (20). For exchange experiments, at least eight different mixing times between 32 ms and 500 ms were used.

Fitting of Kinetic Data. All $^{15}N_z$-exchange data were fit with the program FACSIMILE (36), using an approach similar to that described in ref. 18. For the apparent translocation rates of individual Oct-1 residues (k_{AB}^{app} and k_{BA}^{app}) auto- and cross-peak intensities were fit simultaneously to differential equations describing the time dependence of the magnetizations of the auto- and cross-peaks (Fig. S1*A*) by optimizing four parameters: k_{AB}^{app}, k_{BA}^{app}, R_1 (longitudinal ^{15}N relaxation rates for complexes A and B), and a scale factor S_A for complex A. The scale factor S_B for complex B is given by $S_A(k_{AB}^{app}/k_{BA}^{app})$.

At each temperature in Fig. 2*C*, data for all of the POU_S residues (and similarly for all of the POU_{HD} residues) were fit to one set of apparent k_{AB}^{app} and k_{BA}^{app}, but independent R_1 and S_A values were optimized for each residue. For example, for the POU_S domain at 30°C, 63 data points (27 for F54 and 18 each for S60 and L67) were fit by optimizing 8 parameters: k_{AB}^{app}, k_{BA}^{app}, R_1^{F54}, R_1^{S60}, R_1^{L67}, S_A^{F54}, S_A^{S60}, and S_A^{L67}.

For the DNA concentration-dependent experiments, we chose to analyze the $^{15}N_z$-exchange data for S60 and K106 because these residues had cross-peak and autopeak intensities with significantly higher signal-to-noise than the other three residues at all five DNA concentrations. The $^{15}N_z$-exchange data for these two residues provide 308 time-dependent intensities for fitting to 16 parameters. The data for both domains were fit simultaneously to a model incorporating both intersegmental and jumping pathways as shown in Fig. 3. This scheme has global dissociation constants, k_{off}^{A} and k_{off}^{B}, and domain specific second-order rate constants, k_{AB}^{S*} and k_{BA}^{HD*} for exchange from A to B and k_{BA}^{S*} and k_{BA}^{HD*} for exchange from B to A (for details of the model, see Fig. S1).

ACKNOWLEDGMENTS. We thank Jeong-Yong Sun for assistance with sample preparation. This work was supported by the Intramural Program of the National Institute of Diabetes and Digestive and Kidney Diseases/National Institutes of Health (NIDDK/NIH) and the AIDS Targeted Antiviral Program of the Office of the Director of the NIH (to G.M.C.). M.D was supported by a Nancy Nossal NIDDK/NIH Research Fellowship.

1. Riggs AD, Bourgeois S, Cohn M (1970) The *lac* repressor–operator interaction. 3. Kinetic studies. *J Mol Biol* 53:401–417.
2. Zhou HX, Szabo (2004) Enhancement of association rates by nonspecific binding to DNA and cell membranes. *Phys Rev Lett* 93:178101.
3. Halford SE, Szczelkun MD (2002) How to get from A to B: Strategies for analysing protein motion on DNA. *Eur Biophys J* 31:257–267.
4. Berg OG, von Hippel PH (1985) Diffusion-controlled macromolecular interactions. *Annu Rev Biophys Biophys Chem* 14:131–160.
5. Hu T, Shklovskii BI (2007) How a protein searches for its specific site on DNA: The role of intersegment transfer. *Phys Rev E Stat Nonlin Soft Matter Phys* 76:051909.
6. Berg OG, Winter RB, von Hippel PH (1981) Diffusion-driven mechanisms of protein translocation on nucleic acids. 1. Models and theory. *Biochemistry* 20:6929–6948.
7. von Hippel PH, Revzin A, Gross CA, Wang AC (1975) *Protein–Ligand Interactions*, eds Sund H, Blauer G (Walter de Gruyter, Berlin), pp 278–288.
8. Elf J, Li GW, Xie XS (2007) Probing transcription factor dynamics at the single-molecule level in a living cell. *Science* 316:1191–1194.
9. Blainey PC, van Oijen AM, Banerjee A, Verdine GL, Xie XS (2006) A base-excision DNA-repair protein finds intrahelical lesion bases by fast sliding in contact with DNA. *Proc Natl Acad Sci USA* 103:5752–5757.
10. Iwahara J, Clore GM (2006) Detecting transient intermediates in macromolecular binding by paramagnetic NMR. *Nature* 440:1227–1230.
11. Gowers DM, Wilson GG, Halford SE (2005) Measurement of the contributions of 1D and 3D pathways to the translocation of a protein along DNA. *Proc Natl Acad Sci USA* 102:15883–15888.
12. Iwahara J, Zweckstetter M, Clore GM (2006) NMR structural and kinetic characterization of a homeodomain diffusing and hopping on nonspecific DNA. *Proc Natl Acad Sci USA* 103:15062–15067.
13. Lieberman BA, Nordeen SK (1997) DNA intersegment transfer: How steroid receptors search for a target site. *J Biol Chem* 272:1061–1068.
14. Fried MG, Crothers DM (1984) Kinetics and mechanism in the reaction of gene regulatory proteins with DNA. *J Mol Biol* 172:263–282.
15. Perrin CL, Dwyer TJ (1990) Application of two-dimensional NMR to kinetics of chemical exchange. *Chem Rev* 90:935–967.

16. Di Rocco G, *et al.* (2001) The recruitment of SOX/OCT complexes and the differential activity of HOXA1 and HOXB1 modulate the Hoxb1 autoregulatory enhancer function. *J Biol Chem* 276:20506–20515.
17. Andersen B, Rosenfeld MG (2001) POU domain factors in the neuroendocrine system: Lessons from developmental biology provide insights into human disease. *Endocr Rev* 22:2–35.
18. Iwahara J, Clore GM (2006) Direct observation of enhanced translocation of a homeodomain between DNA cognate sites by NMR exchange spectroscopy. *J Am Chem Soc* 128:404–405.
19. Verrijzer CP, *et al.* (1992) The DNA-binding specificity of the bipartite POU domain and its subdomains. *EMBO J* 11:4993–5003.
20. Sahu D, Clore GM, Iwahara J (2007) TROSY-based *z*-exchange spectroscopy: Application to the determination of the activation energy for intermolecular protein translocation between specific sites on different DNA molecules. *J Am Chem Soc* 129:13232–13237.
21. Milev S, Bosshard HR, Jelesarov I (2005) Enthalpic and entropic effects of salt and polyol osmolytes on site-specific protein-DNA association: The integrase Tn916–DNA complex. *Biochemistry* 44:285–293.
22. Zhou HX (2001) Disparate ionic-strength dependencies of on and off rates in protein–protein association. *Biopolymers* 59:427–433.
23. McConnell HM (1958) Reaction rates by nuclear magnetic resonance. *J Chem Phys* 28:430–431.
24. Williams DC, Jr, Cai M, Clore GM (2004) Molecular basis for synergistic transcriptional activation by Oct1 and Sox2 revealed from the solution structure of the 42-kDa Oct1·Sox2·Hoxb1–DNA ternary transcription factor complex. *J Biol Chem* 279:1449–1457.
25. Klemm JD, Pabo CO (1996) Oct-1 POU domain–DNA interactions: Cooperative binding of isolated subdomains and effects of covalent linkage. *Genes Dev* 10:27–36.
26. Privalov PL, *et al.* (2007) What drives proteins into the major or minor grooves of DNA? *J Mol Biol* 365:1–9.
27. Gumucio DL, *et al.* (1988) Nuclear proteins that bind the human γ-globin gene promoter: Alterations in binding produced by point mutations associated with hereditary persistence of fetal hemoglobin. *Mol Cell Biol* 8:5310–5322.
28. Liu LR, *et al.* (2005) T to C substitution at −175 or −173 of the γ-globin promoter affects GATA-1 and Oct-1 binding *in vitro* differently but can independently reproduce the hereditary persistence of fetal hemoglobin phenotype in transgenic mice. *J Biol Chem* 280:7452–7459.
29. Klemm JD, Rould MA, Aurora R, Herr W, Pabo CO (1994) Crystal structure of the Oct-1 POU domain bound to an octamer site: DNA recognition with tethered DNA-binding modules. *Cell* 77:21–32.
30. Remenyi A, *et al.* (2003) Crystal structure of a POU/HMG/DNA ternary complex suggests differential assembly of Oct4 and Sox2 on two enhancers. *Genes Dev* 17:2048–2059.
31. Oh IH, Reddy EP (1999) The *myb* gene family in cell growth, differentiation, and apoptosis. *Oncogene* 18:3017–3033.
32. Wolfe SA, Nekludova L, Pabo CO (2000) DNA recognition by Cys_2His_2 zinc finger proteins. *Annu Rev Biophys Biomol Struct* 29:183–212.
33. Delaglio F, *et al.* (1995) NMRPipe: A multidimensional spectral processing system based on UNIX pipes. *J Biomol NMR* 6:277–293.
34. Salzmann M, Pervushin K, Wider G, Senn H, Wuthrich K (1998) TROSY in triple-resonance experiments: New perspectives for sequential NMR assignment of large proteins. *Proc Natl Acad Sci USA* 95:13585–13590.
35. Clore GM, Gronenborn AM (1991) Structures of larger proteins in solution: Three- and four-dimensional heteronuclear NMR spectroscopy. *Science* 252:1390–1399.
36. Chance EM, Curtis AR, Jones IP, Kirby CR (1979) FACSIMILE: A computer program for flow and chemistry simulation and general initial value problems (Harwell, HM Stationery Office, London), Atomic Energy Research Establishment Rep R8775.